Published in final edited form as:
IEEE Trans Biomed Eng. 2008 April ; 55(4): 1457–1460. doi:10.1109/TBME.2007.912430.

The Dependence of Spectral Impedance on Disc Microelectrode Radius

Ashish K. Ahuja[*],
Department of Electrical Engineering, Viterbi School of Engineering, University of Southern California, 1355 San Pablo Street, Suite 100, Los Angeles, CA 90033 USA

Matthew R. Behrend,
Department of Electrical Engineering, Viterbi School of Engineering, University of Southern California, Los Angeles, CA 90089 USA

John J. Whalen III,
Doheny Eye Institute, Department of Ophthalmology, Keck School of Medicine, University of Southern California, Los Angeles, CA 90033 USA (jwhalen@amt-med.com)

Mark S. Humayun, and
Doheny Eye Institute, Department of Ophthalmology, Keck School of Medicine, University of Southern California, Los Angeles, CA 90033 USA, and also with the Department of Biomedical Engineering, Viterbi School of Engineering, University of Southern California, Los Angeles, CA 90089 USA (mhumayun@doheny.org; jweiland@doheny.org)

James D. Weiland
Doheny Eye Institute, Department of Ophthalmology, Keck School of Medicine, University of Southern California, Los Angeles, CA 90033 USA, and also with the Department of Biomedical Engineering, Viterbi School of Engineering, University of Southern California, Los Angeles, CA 90089 USA (mhumayun@doheny.org; jweiland@doheny.org)

Abstract

As microelectrodes gain widespread use for electrochemical sensing, biopotential recording, and neural stimulation, it becomes important to understand the dependence of electrochemical impedance on microelectrode size. It has been shown mathematically that a disc electrode, coplanar in an insulating substrate and exposed to a conducting media, exhibits an inhomogeneous current distribution when a potential step is applied. This distribution is known as the primary distribution, and its derivation also yielded an analytic solution for electrical resistance of the conducting media (R_s), between the disc surface and a distant ground, which is inversely proportional to disk radius [$R_s = 1/(4kr)$, where k is media conductivity and r is disk radius]. The dependence of spectral impedance on microelectrode radius, however, has not been explored. We verify the analytical solution for resistance using high-frequency (100 kHz) electrochemical impedance data from microelectrodes of varying radius (11–325 μm). For all disc radii, as we approach a lower frequency ($\rightarrow$10 Hz), we observe a transition from radial to area dependence (e.g., $1/r \rightarrow 1/r^2$). We hypothesize that this transition is driven by the fact that the derivation of the primary distribution ignores concentration gradients, but that these gradients cannot be ignored at lower frequencies.

[*]*corresponding author*. (ashishah@usc.edu). .

Keywords

Electrochemical sensing; impedance spectroscopy; microelectrode; neural stimulation; primary current distribution

I. INTRODUCTION

Advances in photolithography have allowed for the fabrication of microelectrodes for the purposes of impedance-based sensing [1], [2], neurotransmitter detection [3], [4], and neural prosthesis applications [5]-[9]. As these technologies advance they require smaller microelectrodes so that smaller groups of neurons can be individually addressed. Here, we fully characterize the dependence of electrode impedance on electrode size as a function of frequency using microfabricated multielectrode arrays (MEAs) consisting of disc electrodes with varying radii (11–325 μm), and electrochemical impedance spectroscopy (EIS).

Immediately after application of a current or voltage step, an electrode exhibits a nonuniform current distribution known as the primary distribution, which is known to cause preferential corrosion at the electrode edge. This has been proven analytically numerous times by making the assumption that concentration gradients can be ignored [10]-[14]. Upon making this assumption, the equation to be solved is the Laplace equation $\nabla^2 v = 0$ under the following boundary conditions: $v = v_O$ at the electrode surface, $\partial v/\partial z = 0$ at the surface of the insulator, and the fields must approach zero at infinity. Newman was the first to derive the relationship between the solution resistance R_s and electrode radius r to be $R_s = 1/(4kr)$, where k is conductivity [10]. However, the empirical evidence for its veracity over a range of microelectrode radii has not been completed to the best of our knowledge. This has been in part because of the difficulty of fabricating stable microelectrodes with known size and shape [15]-[17]. We confirm Newman's results over various sized microelectrodes using photolithographically fabricated Pt microelectrode discs of varying radius and EIS characterization. We show how impedance does scale inversely with radius (i.e., it follows Newman's relationship) in the high-frequency regime (~100 kHz). However, the impedance transitions from radial dependence to area dependence as the frequency is decreased to 10 Hz. Moreover, smaller microelectrodes (<50 μm), have an RC time constant small enough to exhibit area dependence even at relatively high frequencies of 100 kHz (i.e., frequencies at which larger electrodes are in a solution resistance regime.) By analyzing data at various frequencies we are able to characterize this transition.

II. Experimental

Platinum microelectrodes of varying size were fabricated in parallel on the same float glass substrates (Fig. 1). Two groups, each containing 14 microelectrodes, were fabricated on each substrate; the radii of the microelectrodes were 11, 25, 50, 150, 175, 200, 225, 250, 275, 300, and 325 μm. The details of the two photomask microfabrication process flow are described elsewhere [18]. The trace length was kept constant (26±1.5 mm) for all electrodes and the associated resistance of the platinum traces was 81.0 ± 1.6 Ω.

Electrochemical properties of the microelectrode–electrolyte interface were characterized using impedance spectroscopy. Potentiostatic impedance spectra from 100 kHz to 10 mHz [U = 0.0 V versus open circuit, ΔU = +/− 10-mV root mean square (rms) where U is potential (V)] were collected using a Gamry FAS1 potentiostat (Gamry Instruments, Warminster, PA). Experiments were performed in phosphate buffered saline (PBS) solution to mimic biological chemistry (9-g/L sodium chloride, 0.8-g/L sodium phosphate diabasic, and 0.14-g/L potassium phosphate monobasic) at room temperature and in a Faraday cage.

Electrode potentials were measured with respect to a Ag/AgCl reference electrode and the open circuit potential varied between 0.09 and 0.20 V for the microelectrodes tested. A platinum mesh counter electrode was used for all experiments, and was suspended approximately 2 cm above the MEA in a custom-made Teflon electrochemical cell.

III. Results and Discussion

Except for the three smallest microelectrodes, the impedance magnitude was frequency independent and had the lowest value over the frequency range from 30 to 100 kHz (Fig. 2). At frequencies below 30 kHz, the impedance magnitude increased with decreasing frequency and the phase angle value shifted towards −90°. These changes are indicative of a transition towards capacitive charging processes at the electrode surface.

Radius affected the impedance response of microelectrodes over the entire frequency range tested. The frequency-independent range steadily decreased from 10–100 kHz for the 325-μm radius microelectrode, to 30–100 kHz for the 100-μm radius microelectrode. The three smallest microelectrodes showed no frequency-independent response over the high-frequency range tested. The capacitive charging region of the impedance magnitude showed a shift to higher frequencies with decreasing microelectrode size. This observation has been qualitatively observed in comparing electrodes of different surface area [19], [20].

Impedance measured at 100 kHz was taken as the empirical solution resistance R_s, except as noted here. It is commonly accepted that the high-frequency, frequency-independent impedance response of a microelectrode is attributable to the solution resistance of the electrochemical interface [21]. Additionally, the phase angle at this frequency is typically near or equal to zero. In the case of the three smallest microelectrodes ($\leq$50 μm) the phase angle remained greater than 20° . This result is expected due to the smaller RC time constants of these electrodes, as will be discussed. However, for the purposes of estimating the solution resistance, a phase shift closer to zero was required (i.e., $[\partial|Z|/\partial f]_{100\ \mathrm{KHz}} \approx 0$). To minimize error in approximating R_s for microelectrodes at these radii, impedance data were replotted in the complex plane (data not shown). Z_{img} versus Z_{real} (Nyquist) plots of impedance for platinum microelectrodes in solution have a semicircular shape, with the arc of the semicircle becoming more or less depressed depending on frequency dispersion effects caused by the ionic composition of the solution [22]. The high-frequency intercept of the semicircle is equal to R_s. Here, the high-frequency data was linearly extrapolated to approximate the solution resistance. The values obtained using this extrapolation method differ from the actual impedance value at 100 kHz by less than 3%. R_s values for all microelectrodes are plotted versus radius in Fig. 3.

Microelectrodes have received much interest for electrochemical sensing in large part because of their ability to reach steady state quickly compared with larger electrodes [15]-[17]. The RC time constant is given by $\tau = R_s C = \pi r C_o / 4k$, where R_s is the solution resistance, C is the double-layer capacitance, r is the microelectrode disc radius, C_o is the specific double-layer capacitance, and k is the conductivity [17]. The fact that the 11-, 25-, and 50-μm radius electrodes show fairly capacitive behavior at 100 kHz (e.g., phase angles of 59.3°±2.96°, 46.2°±2.30°, 26.28°±1.31°, respectively) is consistent with the dependence of charging time constant on radius.

As the radius is decreased, the double layer is charged faster, and, therefore, even at the highest measured frequency, τ is less than the period of the sinusoidal voltage perturbation. For example, assuming $k = 1.54$ S/m and $C_o = 20\ \mu\mathrm{F/cm}^2$, then $\tau = 1.12\ \mu$s for the 11-μm radius electrode. Considering that the period at 100 kHz is 10 μs, we can expect that the double layer should be fully charged and discharged even at this frequency. Because there is

a linear relationship between τ and microelectrode disc radius, we expect that an electrode with radius of 125 μm (τ=12.80 μs) would not fully charge the double layer at this frequency, and that is indeed what we observe as the phase of this electrode and the phases of those of greater diameter are <20° at 100 kHz (Fig. 4).

Data were analyzed from 10 Hz to 100 kHz in decade increments and corresponding |Z| versus radius plots were obtained at each of these frequencies (Fig. 3). Three different sets of Pt microelectrode discs of varying radius were characterized for the purposes of repeatability. The arithmetic means of the three data sets were then plotted and a power series curve fit was used to determine the functional form of this average (r > 0.99 for all curve fits).We see good correspondence for all of these electrode sets (average standard deviations for all three MEAs over all electrode sizes are 28.9%, 14.2%, 19.0%, 18.4%, and 16.7% for 10 Hz, 100 Hz, 1 kHz, 10 kHz, and 100 kHz data sets, respectively). We noted excellent correspondence between our own measured dependence of R_s on microelectrode radius and Newman's analytically derived function (mean deviation 6.26% ± 3.40%), and there is a gradual transition from approximately a $1/R$ dependence (i.e., $1/R^{1.05}$) to approximately a $1/R^2$ dependence (i.e., $1/R^{1.97}$) as frequency decreases from 100 kHz to 10 Hz. At 10 kHz, for an electrode radius range of 11-325 μm, we observe a $1/R^{1.56}$ dependence indicating that most of the electrodes are largely in area-driven regime within one decade of frequency from the solution-resistive regime.

We believe that the physical basis for this transition is as follows. As the frequency decreases, there is a longer time available for a given electrode to reach the steady state. As the time of anodic/cathodic bias is increased, the assumption made in Newman's derivation of the primary distribution no longer holds for two reasons: 1) the solution side of the double layer is no longer isopotential as it charges, and 2) concentration gradients arise due to carrier depletion. When the period of the perturbation is long compared to the electrode time constant, a more uniform charging over the surface takes place. This is consistent with the fact that the exact solution of the primary distribution predicts singularities at the electrode that are, clearly, not physically achievable. Indeed, concentration gradients must be taken into account to realize a physically meaningful solution [10]-[14]. Because reactants are preferentially consumed at the electrode periphery, a nonuniform concentration gradient forms across the electrode surface. Once these effects are taken into account, the known secondary current distribution results [23]. Because of this effect, we expect some transition to area-dependent impedance as the period of the sinusoidally varying voltage approaches the RC time constant for a microelectrode of a specific radius, and as the capacitive double layer is charged.

IV. Conclusion

The dependence of impedance on microelectrode size and radius has been investigated by fabricating arrays of varying radius Pt thin-film electrodes. Fourteen different sizes have been investigated, having radii ranging from 11 to 325 μm. EIS was used to extract the dependence of impedance magnitude and phase on microelectrode disc diameter and perturbation frequency.We empirically confirmed Newman's relationship for the dependence of solution resistance (i.e., high-frequency impedance).

The phase data taken from the same analysis show that the smaller microelectrodes (≤50 μm) are in an area-driven capacitive regime at the same frequency (100 kHz) that larger electrodes are in a solution-resistive regime. This is due to the decreased RC time constant of the smaller microelectrodes and to the fact that they exhibit double layer charging at these frequencies. The fact that the time constant for these electrodes is less than the period of the sinusoidally varying voltage at this frequency confirms this fact. The dependence of

impedance on diameter is investigated over five decades of frequency. By using a power series fit on data collected from three different microelectrode arrays we observe that a steady transition is made from approximately $1/r$ to $1/r^2$ dependence as the frequency is tuned from 100 kHz to 10 Hz.We believe that the primary current distribution depletes carriers preferentially at the electrode perimeter. As this process evolves, a concentration gradient is formed at the periphery with respect to the center. This effect, known as the secondary current distribution, will drive current to the center of the disk thereby yielding area dependence.

With regards to neural stimulation, the dependence of electrode current distribution on frequency suggests a method of controlling the excitation area by modifying stimulus pulse shape. The lower order harmonics (or frequency components) define the pulse frequency while the higher order harmonics determine how well the pulse edges mimic an ideal square wave. Taken together with results presented here, this suggests that at the onset of a stimulus square pulse the current is delivered primarily at the electrode edge, and this distribution evolves during the time course of the pulse to include the electrode center. Therefore, a sin wave stimulus delivering the same amount of total charge as a square wave stimulus would likely excite a greater population of cells in the electrode center since it does not consist of the higher order harmonics present in the latter. It is interesting to note that early cortical stimulation studies used sin wave stimuli [24], [25], and it has been shown in isolated retina stimulation that sin wave pulses have a lower threshold for stimulation compared with square wave pulses of the same amplitude [26].

Acknowledgments

This work was supported in part by the National Science Foundation under Grant EEC-0310723 and the Department of Energy under Grant DE-FC02-04ER63735. The work of M. Behrend was supported by the Fannie and John Hertz Foundation and the National Defense Science & Engineering Fellowship.

References

[1]. Wegener J, Keese CR, Giaever I. Electric cell-substrate impedance sensing (ECIS) as a noninvasive means to monitor the kinetics of cell spreading to artificial surfaces. Exp. Cell Res. 2000; 259:158–166. [PubMed: 10942588]

[2]. Yang L, Ruan C, Li Y. Detection of viable Salmonella ty- phimurium by impedance measurement of electrode capacitance and medium resistance. Biosens. Bioelectron. 2003; 19:495–502. [PubMed: 14623474]

[3]. Stamford JA. Fast cyclic voltammetry: Measuring transmitter re- lease in ‘real time’. J. Neurosci. Methods. 1990; 34:67–72. [PubMed: 1979652]

[4]. Stamford JA. In vivo voltammetry—Prospects for the next decade. Trends Neurosci. 1989; 12:407–412. [PubMed: 2479139]

[5]. Parent A, Giovanni A. Giovanni Aldini: From animal electricity to human brain stimulation. Can. J. Neurol. Sci. 2004; 4:576–584. [PubMed: 15595271]

[6]. Robblee, LS.; Rose, TL. Neural Prosthesis Fundamental Studies. Agnew, WF.; McCreery, DB., editors. Pren- tice-Hall; Englewood Cliffs, NJ: 1990. ch. 2

[7]. Loeb, GE. Neural Prosthetics: Handbook of Brain Theory and Neural Networks. 2nd ed.. Arbib, MA., editor. MIT Press; Cambridge, MA: 2002.

[8]. Humayun MS, DeJaun E Jr. Weiland JD, Dagnelie G, Katona S, Greenberg RJ, Suzuki S. Pattern electrical stimulation of the human retina. Vis. Res. 1999; 39:2569–2576. [PubMed: 10396625]

[9]. Weiland JD, Liu W, Humayun MS. Retinal prosthesis. Annu. Rev. Biomed. Eng. 2005; 7:361–401. [PubMed: 16004575]

[10]. Newman JS. Resistance for flow of current to a disk. J. Elec- trochem. Soc. 1966; 113(5):501–502.

[11]. Wagner C. Theoretical analysis of the current distribution in elec- trolytic cells. J. Electrochem. Soc. 1951; 98:116–119.

[12]. Wiley JD, Webster JG. Analysis and control of the current distribution under circular dispersive electrodes. IEEE Trans. Biomed. Eng. May; 1982 BME-29(5):381–385. [PubMed: 7084970]

[13]. Wiley JD, Webster JG. Distributed equivalent circuit models for circular dispersive electrodes. IEEE Trans. Biomed. Eng. May; 1982 BME-29(5):385–389. [PubMed: 7084971]

[14]. Rubinstein JT, Spelman FA, Soma M, Suesserman MF. Cur- rent density profiles of surface mounted and recessed electrodes for neural prostheses. IEEE Trans. Biomed. Eng. Nov; 1987 BME-34(11):864–875. [PubMed: 3319885]

[15]. Stulik K, Amatore C, Holub K, Marecek M, Kutner W. Micro- electrodes: Definitions, characterization, and applications. Pure App. Chem. 2000; 72(8):1483–1492.

[16]. Oldham KB. Steady-state voltammetry at microelectrodes of arbi- trary shape. J. Electroanal. Chem. 1992; 323:53–76.

[17]. Sandison ME, Anicet N, Glidle A, Cooper JM. Optimiza- tion of the geometry and porosity of microelectrode arrays for sensor design. Anal. Chem. 2002; 74:5717–5725. [PubMed: 12463354]

[18]. Gholmieh G, Soussou W, Han M, Ahuja AK, Hsiao MC, Song D, Wang Z, Tanuay AR Jr. Berger TW. Custom-designed high- density conformal planar multielectrode arrays for brain slice electro- physiology. J. Neurosci. Meth. 2006; 141(1):391–406.

[19]. Franks W, Schenker I, Schmutz P, Hierlemann A. Impedance characterization and modeling of electrodes for biomedical applica- tions. IEEE Trans. Biomed. Eng. Jul; 2005 52(7):1295–1302. [PubMed: 16041993]

[20]. Bard, AJ.; Faulkner, LR. Electrochemical Methods. Wiley; New York: 1980.

[21]. Duan YY, Clark GM, Cowan RSC. Factors determining and limiting the impedance behavior of implanted bioelectrodes. Proc. SPIE: Smart Structures Devices. 2001; 4235:498–508.

[22]. Mailley S, Hyland M, Mailley P, McLaughlin JA, McAdams ET. Thin film platinum cuff electrodes for neurostimulation: In vitro approach of safe neurostimulation parameters. Bioelectro- chemistry. 2004; 63:359–364.

[23]. Heitz, E.; Kreysa, G. Principles of Electrochemical Engineering. VCH; New York: 1996.

[24]. Brindley GS, Lewin WS. The sensations produced by electrical stimulation of the visual cortex. J. Physiol. 1968; 196:479–493. [PubMed: 4871047]

[25]. Brindley GS, Rushton D. Implanted stimulators of the visual cortex as visual prosthetic devices. Trans. Amer. Acad. Ophthalmol. Otolaryngol. 1974; 78:741–745.

[26]. Suzuki S, Humayun MS, Weiland JD, Chen SJ, Margalit E, Piyathaisere DV, de Juan E Jr. Comparison of electrical stimula- tion thresholds in normal and retinal degenerated mouse retina. Jpn. J. Ophthalmol. 2004; 48:345–349. [PubMed: 15295659]

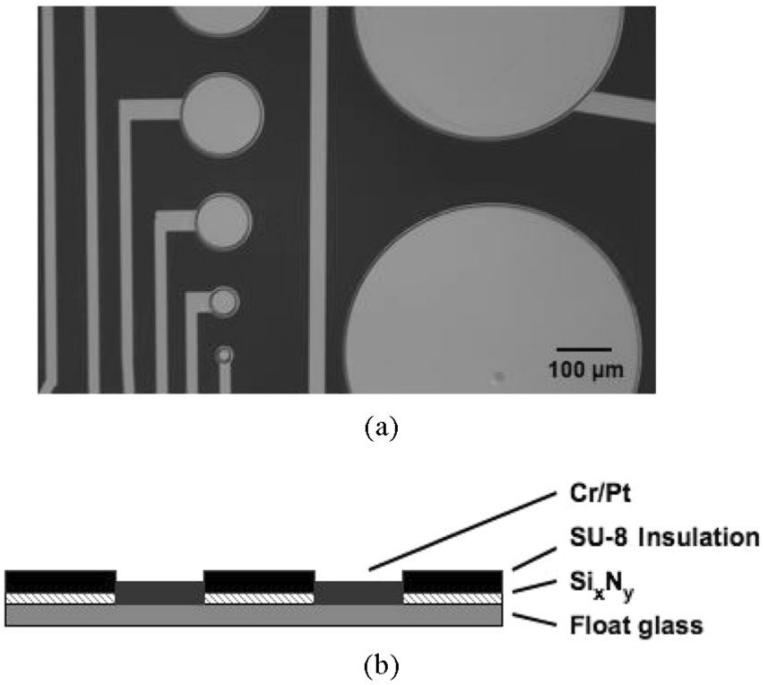

Fig. 1.
(a) Photolithographically fabricated Pt MEA with varying disk radius. (b) Corresponding cross-sectional schematic.

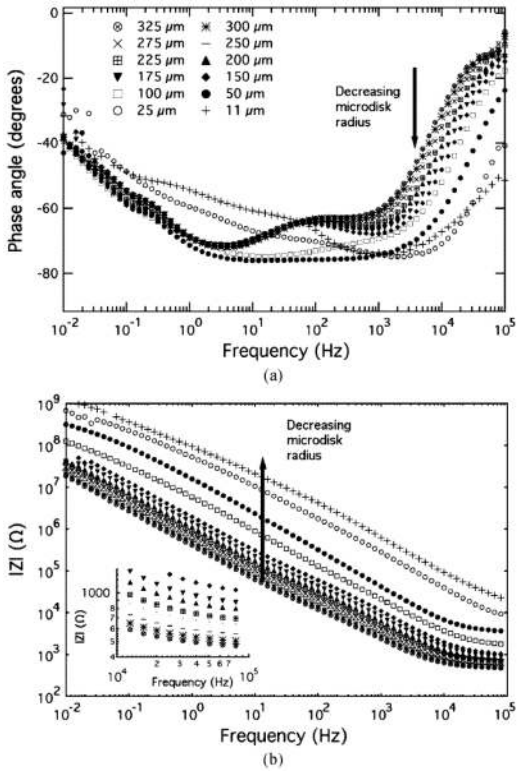

Fig. 2.

(a) Phase angle versus frequency. (b) $|Z|$ versus frequency for Pt microdiscs of varying diameter in phosphate buffered saline. (Inset) Magnification of high-frequency range of eight largest electrodes.

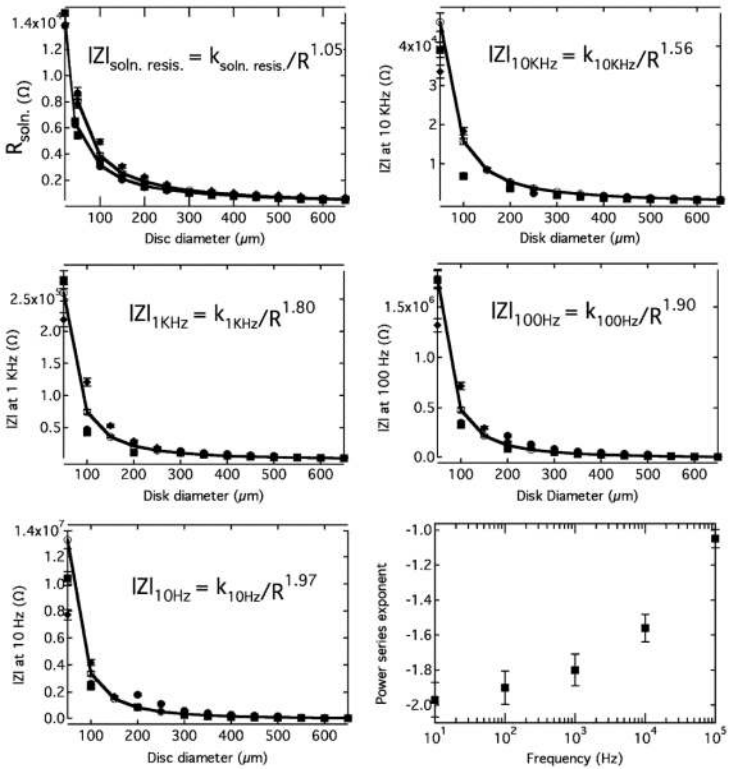

Fig. 3.

|*Z*| versus microdisc radius at 100 kHz, 10 kHz, 1 kHz, 100 Hz, and 10 Hz in PBS and corresponding power series curve fits for three different sets of variable sized microdiscs. (Bottom right) Power series fit exponent versus frequency indicating shift to area dependence of impedance at lower frequencies.

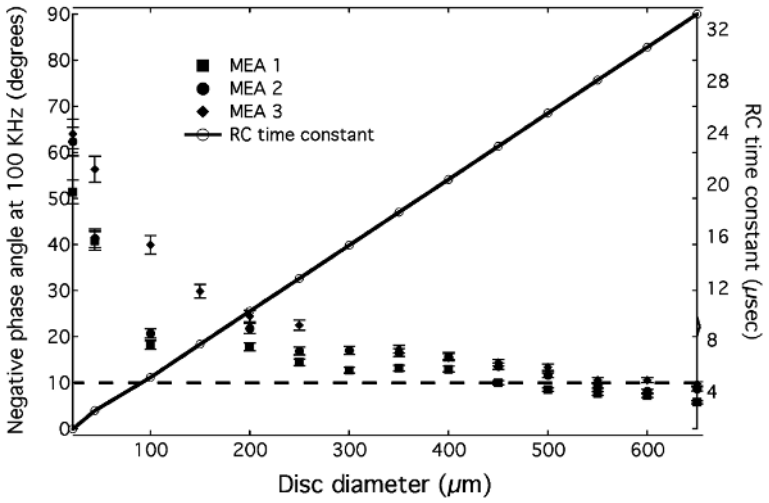

Fig. 4.

(Left axis) Phase shift at 100 kHz versus microdisc radius for three different electrode arrays showing how smaller electrodes behave largely capacitively compared with larger electrodes. (Right axis) Time constant versus disc diameter. The dashed line indicates half the period of the sinusoidally varying voltage at 100 kHz.